diversity

MDPI

Article

Semicryptic Diversity around *Chaetoceros elegans* (Bacillariophyta, Mediophyceae), and the Description of Two New Species

Xiumei Chen [1], Zuoyi Chen [1,2], Nina Lundholm [3], Sing Tung Teng [4], Xiaojing Xu [1] and Yang Li [1,*]

[1] Guangzhou Key Laboratory of Subtropical Biodiversity and Biomonitoring, Guangdong Provincial Key Laboratory for Healthy and Safe Aquaculture, College of Life Science, South China Normal University, Guangzhou 510631, China
[2] The Eighth Geological Brigade, Hebei Geological Prospecting Bureau, Qinhuangdao 066001, China
[3] Natural History Museum of Denmark, University of Copenhagen, Øster Farimagsgade 5, 1353 Copenhagen, Denmark
[4] Faculty of Resource Science and Technology, Universiti Malaysia Sarawak, Kota Samarahan 94300, Malaysia
* Correspondence: li-3-yang@163.com

Abstract: The globally distributed *Chaetoceros elegans* belongs to the *Chaetoceros lorenzianus* (*C. lorenzianus*) complex and is characterized by having tear-shaped setae poroids. Several strains of *C. elegans* were established from Chinese coastal waters. The vegetative cells and the resting spores were observed using light and electron microscopy. Phylogenetic analyses of two nuclear ribosomal RNA genes (SSU and the D1–D3 region of LSU) and the internal transcribed spacer (ITS) revealed that the *C. elegans* strains clustered into three clades, corresponding to different morphotypes. Based on the type material, the delineation of *C. elegans* was amended, and two new taxa, (*Chaetoceros macroelegans*) *C. macroelegans* sp. nov. and (*Chaetoceros densoelegans*) *C. densoelegans* sp. nov., were described. The two new taxa are featured by the presence of two types of setae poroids, tear-shaped and round-oval setae poroids, whereas only tear-shaped setae poroids are seen in *C. elegans*. The setae base is distinct in *C. elegans*, but absent or short in the two new taxa. In *C. macroelegans*, the tear-shaped poroids on the intercalary setae are larger and less densely spaced than in the other two species. The round-oval setae poroids are more densely spaced in *C. densoelegans* than in *C. macroelegans*, although they have more or less the same size. Resting spores characterize the two new taxa, but are unknown in the amended *C. elegans*. When comparing the ITS2 secondary structure, two and four compensatory base changes (CBCs) distinguish *C. elegans* from *C. macroelegans* and *C. densoelegans*, respectively. Between the two new taxa, no CBC but five hemi-CBCs (HCBCs) are present. The shape, size and density of the setae poroids, as well as the morphology of the resting spores, are important characteristics for species identification among the presently nine known species within the *C. lorenzianus* complex.

Keywords: setae poroid; resting spore; phylogeny; *Chaetoceros elegans*; *C. macroelegans*; *C. densoelegans*

Citation: Chen, X.; Chen, Z.; Lundholm, N.; Teng, S.T.; Xu, X.; Li, Y. Semicryptic Diversity around *Chaetoceros elegans* (Bacillariophyta, Mediophyceae), and the Description of Two New Species. *Diversity* **2022**, *14*, 676. https://doi.org/10.3390/d14080676

Academic Editors: Renhui Li and Wei Zhang

Received: 8 July 2022
Accepted: 16 August 2022
Published: 18 August 2022

1. Introduction

Chaetoceros is one of the most diverse marine planktonic diatom genera, with more than 500 species and infraspecies recorded, and over 200 considered as taxonomically accepted species [1]. Species recognition is normally difficult because a number of the species have been described based on light microscopy only. The delineation of several commonly recorded species has been amended—for example, *C. socialis* [2], *C. compressus* and *C. contortus* [3], *C. debilis* [4]—and new species have also been described [5–10].

Recently, the section *Dicladia*, also called the *C. lorenzianus* complex, was explored, and the delineations of *C. decipiens*, *C. mitra* and *C. lorenzianus* were amended and four new species were described [11,12]. *Chaetoceros elegans*, one of the four new taxa, was characterized by tear-shaped setae poroids, a distinct seta base and the primary valve of resting

spores having two elongated elevations with dichotomously branching processes [11]. Presently, *C. elegans* has been shown to have a wide global distribution comprising the type locality in the South China Sea, several coastal localities in the East China Sea and the Yellow Sea, as well as coastal waters of Thailand, Canada (New Brunswick) and Chile [11,13]. However, differences in the shape of the setae poroids and the presence or absence of a seta base were observed among different strains of *C. elegans* [11]. Shortly afterwards, molecular divergences were found in the analyses inferred from the LSU and SSU rRNA genes [13,14].

In order to clarify whether the morphological and molecular variations comprise so far hidden taxonomic information regarding the delineation of *C. elegans* and related diversity, monoclonal strains belonging to *C. elegans* sensu lato were established. Based on a combination of the morphological features of vegetative cells and resting spores, phylogenetic analyses of nuclear genes and comparisons of the ITS2 secondary structure, the description of *C. elegans* was amended and two new taxa were discovered.

2. Materials and Methods

2.1. Strain Isolates and Maintenance

By hauling a nylon net (10 µm mesh size) horizontally, plankton samples were obtained in several localities along the Chinese shoreline (Table 1). Using a glass micropipette, single cells or chains of *Chaetoceros* similar to the *C. lorenzianus* complex (described in [11]) were isolated by an inverted light microscope (Nikon TMS, Tokyo, Japan) and transferred to a 48-well cell culture plate (Greiner Bio-One GmbH, Frickenhausen, Germany) with each well containing ca. 800 µL L1 medium of the same salinity as the respective sampling locality [15]. The plate was incubated in a 12:12 light:dark (L:D) cycle at 20 ± 2 °C. When the cell abundance reached >100 cells (manually counted), the strains were shifted to glass flasks and numbered as marine collection (MC) series.

Table 1. Strains of *C. elegans*, *C. macroelegans* sp. nov and *C. densoelegans* sp. nov. used in this study, showing strain designation, sampling location and date, as well as ITS, LSU and SSU accession numbers. * represents holotype/means no data.

Species	Strain	Locality	Date	Accession Number		
				LSU	ITS	SSU
C. elegans	YL7 *	Dapeng Bay, 22.5933° N, 114.3991° E	27 August 2010	KX065232	ON972673	ON944143
	MC1048	Dapeng Bay, 22.5953° N, 114.3981° E	30 September 2015	KX065233	ON972674	ON944144
	MC1051	Dapeng Bay, 22.5953° N, 114.3981° E	1 October 2015	ON944163	ON972675	ON944145
C. macroelegans	MC733	Hong Kong, 22.2960° N, 114.1840° E	10 July 2015	ON944164	ON972676	ON944146
	MC732	Hong Kong, 22.2960° N, 114.1840° E	10 July 2015	ON944165	ON972677	ON944147
	MC747	Jiangmen, 21.8361° N, 113.1916° E	5 August 2015	ON944166	ON972678	ON944148
	MC750	Jiangmen, 21.8361° N, 113.1916° E	5 August 2015	ON944167	/	ON944149

Table 1. *Cont.*

Species	Strain	Locality	Date	Accession Number		
				LSU	ITS	SSU
	MC758	Jiangmen, 21.8361° N, 113.1916° E	5 August 2015	ON944168	/	/
	MC761	Jiangmen, 21.8361° N, 113.1916° E	5 August 2015	ON944169	/	ON944150
	MC767	Ningbo, 29.8636° N, 121.5611° E	6 August 2015	ON944170	ON972679	ON944151
	MC777	Ningbo, 29.8636° N, 121.5611° E	7 August 2015	ON944171	ON972680	ON944152
	MC785 *	Ningbo, 29.8636° N, 121.5611° E	7 August 2015	ON944172	ON972681	ON944153
	MC788	Zhuhai, 22.1614° N, 113.3436° E	17 August 2015	KX065236	ON972682	/
	MC790	Zhuhai, 22.1614° N, 113.3436° E	17 August 2015	ON944173	ON972683	/
	MC1000	Zhanjiang, 20.9566° N, 110.3998° E	26 August 2015	ON944174	ON972684	ON944154
	MC1001	Zhanjiang, 20.9566° N, 110.3998° E	26 August 2015	ON944175	ON972685	ON944155
	MC1026	Qingdao, 36.0329° N, 120.3473° E	9 September 2015	ON944176	/	ON944156
	UNBF	New Brunswick, Canada, 45.00° N, 66.733° W	7 September 2010	KC986068	/	/
	M1	Mannai Island, Thailand, 12.6111° N, 101.6836° E	2 June 2008	KXO65231	/	/
C. densoelegans	MC687 *	Hong Kong, 22.3520° N, 114.1139° E	3 April 2015	ON944179	ON972686	ON944157
	MC688	Hong Kong, 22.2960° N, 114.1840° E	3 April 2015	ON944180	ON972687	ON944158
	Ch12A1	Concepción, Chile, 36.5133° S and 73.1291° W	29 October 2013	KY129903	/	KX611421

Induction of resting spore formation was attempted at least three times for each strain by inoculation into L1 medium prepared without nitrate. The remaining culture conditions were the same as above.

2.2. Morphological Observations

Light microscopical (LM) observations were conducted by an Olympus BX53 light microscope (Olympus, Tokyo, Japan) with an Olympus DP27 camera. Preparation of the diatom frustules followed [11]. For transmission electron microscopy (TEM), acid-cleaned frustules were placed on copper grids, air-dried and observed using a JEM-1010 TEM (JEOL Ltd., Tokyo, Japan). For scanning electron microscopy (SEM), acid-cleaned frustules were filtered onto Isopore^{TM} membrane filters, pore size 3 µm (Merck Millipore Ltd., Cork, Ireland). The filters were attached to stubs and sputter-coated for 100 s with gold–palladium in a Polaron E5000 sputter-coater (Gala, Bad Schwalbach, Germany) before examination in a Zeiss Ultra 55 SEM (Zeiss, Oberkochen, Germany).

Key morphometric characteristics, such as the size, density and shape of setae poroids, apical and pervalvar axis, height of aperture in pervalvar axis, length of elevation and process on resting spore, were mainly measured on the EM micrographs. The morphometric data followed a normal distribution, and one-way ANOVA with Bonferroni–Holm post hoc tests were performed using Daniel's XL Toolbox for Excel, version 6.22 [16]. The terminology followed [11,17–20].

2.3. Phylogenetic Analyses Inferred from Nucleic Genes

DNA extraction followed [21]. For each strain, two nuclear ribosomal RNA-encoding genes (SSU and the D1–D3 domain of LSU) and the internal transcribed spacer (ITS) were amplified. The primers D1R-F [22] and D3B-R [23] were used for LSU. The primers SSU-F and SSU-R were used to amplify SSU [24], and primers ITS1 and ITS4 were used for ITS [25]. PCR products were purified using the QIAquick PCR Purification Kit (Qiagen, Hilden, Germany), as recommended by the manufacturer, and sent to BGI Corporation (BGI, Guangzhou, China) for sequencing.

Sequences were blasted, and closely related sequences or sequences of related species were downloaded from GenBank. They were included in the alignment together with the sequences of morphologically allied species, if available. The sequences were aligned and edited using BioEdit [26]. *Chaetoceros dayaensis* was included as an outgroup for the analyses inferred from LSU, SSU and ITS, respectively, based on previous studies [13,14]. The alignments were subjected to Bayesian inference (BI) and maximum likelihood (ML) analyses. ML analyses were conducted by heuristic searches with 10 random addition replicates and the branch-swapping algorithm (TBR, tree-bisection reconnection), using RAxML v7.2.6 [27] on the T-REX web server [28]. One thousand bootstrap replicates were performed in ML. BI analyses were run using MrBayes 3.2 [29]. The optimal models were selected by MrModeltest 2.3 [30].

2.4. ITS2 Secondary Structure Comparison

The ITS2 transcript of *Chaetoceros laevisporus* (ON241763, strain MC746) was modeled and used as an outgroup. The command script is available via 4SALE [31,32]. The CBC Analyzer option in 4SALE was used to analyze compensatory base changes (CBCs). The HCBC (hemi-CBC) was analyzed based on the homologous secondary structure of ITS2 by using the structure viewer feature in 4SALE [33].

3. Results

The phylogenetic trees inferred from two nuclear ribosomal encoding genes (SSU and D1–D3 region of LSU) and the internal transcribed spacer (ITS) showed that the *C. elegans* strains clustered in three clades corresponding to different morphotypes. When comparing the type description and the type material, one clade was assigned to *C. elegans*. The other two clades were described as new taxa, *C. macroelegans* sp. nov. and *C. densoelegans* sp. nov.

Because the description of *C. elegans* in [11] comprised morphological information of strains MC785 and CH12A1 that we here refer to the two new taxa, the description of *C. elegans* was amended based on the morphology of the type material (strain YL7) and other strains (MC1048 and MC1051) belonging to the same clade.

In the amended *C. elegans*, a distinguishing feature is that the intercalary setae extend initially in approximately the direction of the pervalvar axis, before curving and crossing over (Figure 1a,b). This means that the intercalary setae bases are distinct in *C. elegans*, and therefore the apertures are large and rounded quadrangular–rectangular (Figure 1a,b). The setae poroids are tear-shaped on both intercalary and terminal setae (Figure 1c–f), and never round-oval. The size and density of setae poroids are updated with data only belonging to the amended *C. elegans* (see below and Table 1). No resting spores were observed in any of the strains that belong to the amended *C. elegans*. The resting spores described in [11] refer to the two new taxa described below.

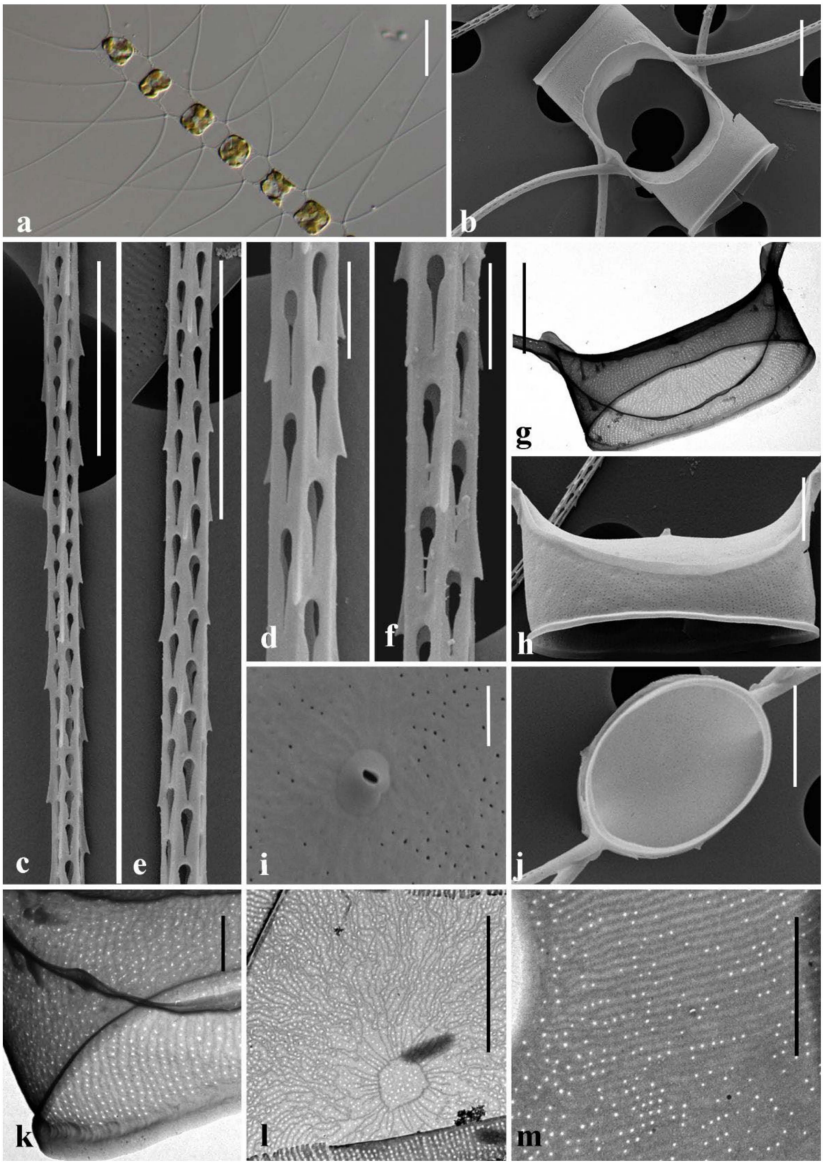

Figure 1. LM (**a**), SEM (**b**–**f**,**h**–**j**) and TEM (**g**,**k**–**m**) micrographs of *Chaetoceros elegans*, strain YL7. (**a**) Chain in broad girdle view; (**b**) sibling intercalary valves showing setae base and aperture; (**c**–**f**) poroids and spines on terminal (**c**,**d**) and intercalary setae (**e**,**f**); (**g**,**h**) terminal valves; (**i**) close-up of rimoportula; (**j**) intercalary valve view; (**k**) rows of poroids on the mantle; (**l**) central annulus on intercalary valve; (**m**) close-up of bands. Scale bars: (**a**) 20 µm; (**b**–**d**,**g**,**h**,**j**,**l**) 5 µm; (**e**,**f**,**i**,**k**,**m**) 1 µm.

3.1. Morphological Description of Three Chaetoceros Species

Chaetoceros elegans Yang Li, Boonprakob, Moestrup & Lundholm emend. Lundholm & Yang Li (Figure 1).

Emended diagnosis: Straight chains, sometimes solitary cells. Usually 4–10 chloroplasts in each cell. Apical axis 9.2–14.7 µm. Pervalvar axis 9.2–16.4 µm. Height of aperture 7.8–12.9 µm. Cells quadrangular in girdle views. Central annulus, radiating costae and scattered poroids on valve face and mantle. Large and rounded, quadrangular–rectangular apertures. Setae Brunel I type. Setae base extending in pervalvar axis. Sibling setae intersect outside chain border. Terminal setae diverge in direction of chain. Four–six-sided setae ornamented by four to six rows of poroids and spines. Tear-shaped setae poroids on both intercalary and terminal setae. A rimoportula on terminal valve. Several bands, each having parallel rows of poroids separated by costae. Resting spores unknown.

Holotype: Glutaraldehyde-fixed material of strain YL7, isolated from Dapeng Bay, deposited at the Natural History Museum of Denmark, Copenhagen (C-A92069). Figure 4A–D in Li et al. 2017 illustrate the holotype.

Isotype: Glutaraldehyde-fixed material of strain YL7 deposited at the Marine Diatoms Collection of South China Normal University, China, catalogue number SN F-YL7.

Type locality: Dapeng Bay (22.5933° N, 114.3991° E), South China Sea.

Emended description: The chains are straight and often comprise 4–8 cells (Figure 1a). Usually 4–10 chloroplasts are present in each cell (Figure 1a). Cells are quadrangular in broad girdle views (Figure 1a). The apertures are large and rounded quadrangular–rectangular (Figure 1a,b).

For each chain, all setae are located in the apical plane (Brunel group I) (Figure 1a). The setae protrude from the cell corners and the setae bases are distinct (Figure 1b). Sibling setae form an acute angle and intersect outside the chain border without fusing (Figure 1a,b). The basal parts of the intercalary setae extend initially in the direction of the pervalvar axis, before curving and crossing over (Figure 1a). Four to six rows of poroids and spines are found on the four–six-sided setae (Figure 1c–f). The poroids on both intercalary and terminal setae are tear-shaped, 0.7 ± 0.2 µm in length and 12.0 ± 3.1 poroids in 10 µm on the intercalary setae, and 0.9 ± 0.2 µm in length and 9.4 ± 1.7 poroids in 10 µm on the terminal setae (n > 100) (Table 2).

Table 2. Morphological comparison among *C. elegans*, *C. macroelegans* sp. nov. and *C. densoelegans* sp. nov. [a,b] indicates statistically significant difference ($p < 0.01$). The most important morphological differences are highlighted in bold.

Characters		*C. macroelegans*	*C. densoelegans*	*C. elegans*
Brunel group		I	I	I
Aperture shape		**elliptical to hexagonal**	**elliptical to hexagonal**	**quadrangular-rectangular**
Poroids on valve face		present	present	present
External tube of rimoportula		short	short	short
Basal part of seta		**absent or short**	**absent or short**	**present, distinct**
Seta poroid shape	Terminal seta	tear-shaped, round-oval	tear-shaped, round-oval	tear-shaped
	Intercalary seta	tear-shaped, round-oval	tear-shaped, round-oval	tear-shaped
Seta poroid size/density (10 µm)	Terminal seta	0.5–1.3 (0.7 ± 0.2) [a] (tear-shaped)/ 6.5–16.0 (11.0 ± 2.2) [a] (tear-shaped) 0.4–0.6 (0.4 ± 0.1) [a] (round-oval)/ **12.0–19.1 (15.8 ± 2.3) [a] (round-oval)**	0.5–0.7 (0.6 ± 0.1) [a] (tear-shaped)/ 9.3–14.2 (12.3 ± 2.7) [a] (tear-shaped) 0.2–0.5 (0.4 ± 0.1) [b] (round-oval)/ **15.0–27.0 (19.5 ± 3.1) [b] (round-oval)**	0.6–1.2 (0.9 ± 0.2) [b]/ 7.2–12.8 (9.4 ± 1.7) [b]

Table 2. *Cont.*

Characters		*C. macroelegans*	*C. densoelegans*	*C. elegans*
	Intercalary seta	**0.7– 2.3 (1.2 ± 0.3) [a] (tear-shaped)/** 5.0–13.0 (7.9 ± 1.7) [a] (tear-shaped) 0.4– 0.5 (0.4 ± 0.03) [a] (round-oval)/ **15.3–18.3 (17.1 ± 1.2) [a] (round-oval)**	**0.6–0.9 (0.7 ± 0.1) [b] (tear-shaped)/** 8.4–14.0 (11.2 ± 2.1) [b] (tear-shaped) 0.3–0.5 (0.4 ± 0.1) [b] (round-oval)/ **13.5–27.0 (20.0 ± 4.2) [b] (round-oval)**	**0.4–1.0 (0.7 ± 0.2) [b]/** 8.0–18.5 (12.0 ± 3.1) [b]
Apical axis (μm)		12.6–39.7 (27.9 ± 10.8)	25.0–26.5 (25.5 ± 0.6)	9.2–14.7 (12.5 ± 1.8)
Pervalvar axis (μm)		11.3–28.4 (17.5 ± 3.9)	9.4–15.8 (12.4 ± 2.2)	9.2–16.4 (12.0 ± 1.7)
Aperture in pervalvar axis (μm)		6.3–12.6 (8.9 ± 2.0)	8.3–14.5 (11.4 ± 1.5)	7.8–12.9 (10.2 ± 2.0)
Aperture height/ pervalvar axis index		0.2–0.7 (0.4 ± 0.1) [a]	0.3–0.6 (0.5 ± 0.1) [b]	0.5–0.9 (0.7 ± 0.1) [b]
Resting spore		two branching processes	two branching processes	unknown
	Apical axis (μm)	20.3–47.1 (33.8 ± 7.2)	18.3–32.9 (28.6 ± 4.2)	
	Pervalvar axis of primary valve (μm)	8.4–16.3 (11.2 ± 2.2)	9.1–13.6 (11.4 ± 1.2)	
	Height of branching processes (μm)	9.5–14.9 (11.4 ± 1.3)	9.6–16.3 (13.3 ± 1.8)	
	Height of elevation (μm)	4.4–10.3 (6.9 ± 1.6)	6.0–9.6 (7.5 ± 1.0)	
	Outer slope of elevation	Acute angle	Acute angle	
	Joining of two elevations	Near mantle	Near mantle	
	Structure of distal tips	Hook	Hook	
	Secondary valve bulges	1–2	1–2	
	Branching times	5–6	5–6	
	Elevations/branching processes	0.4–0.8 (0.6 ± 0.1)	0.4–1.0 (0.6 ± 0.1)	

The valve face edge is broadly arc-shaped and marked by an elevated silica rib (Figure 1b,h). A single rimoportula is situated centrally on the terminal valve (Figure 1h,i), but absent on the intercalary valve (Figure 1j). The valves are elliptical to round-oval (Figure 1j). The valve face is saddle-shaped, with a slightly raised central region (Figure 1b,h). The height of the mantle is nearly one third of the pervalvar axis, and parallel rows of poroids separated by narrow costae are present (Figure 1k). A furrow is seen above the basal ring of the mantle (Figure 1b). On the valve face, costae diverge from a central annulus, with poroids scattered in between (Figure 1l). Several open girdle bands are present, each ornamented with single rows of scattered poroids separated by parallel costae (Figure 1m). The length of the apical axis is 9.2–14.7 μm, the pervalvar axis 9.2–16.4 μm, and the height of the apertures in the pervalvar axis is 7.8–12.9 μm (Table 2).

Resting spores unknown.

Geographical distribution: Dapeng Bay, South China Sea (present study, [11]).

Chaetoceros macroelegans X. M. Chen & Yang Li sp. nov. (Figures 2 and 3).

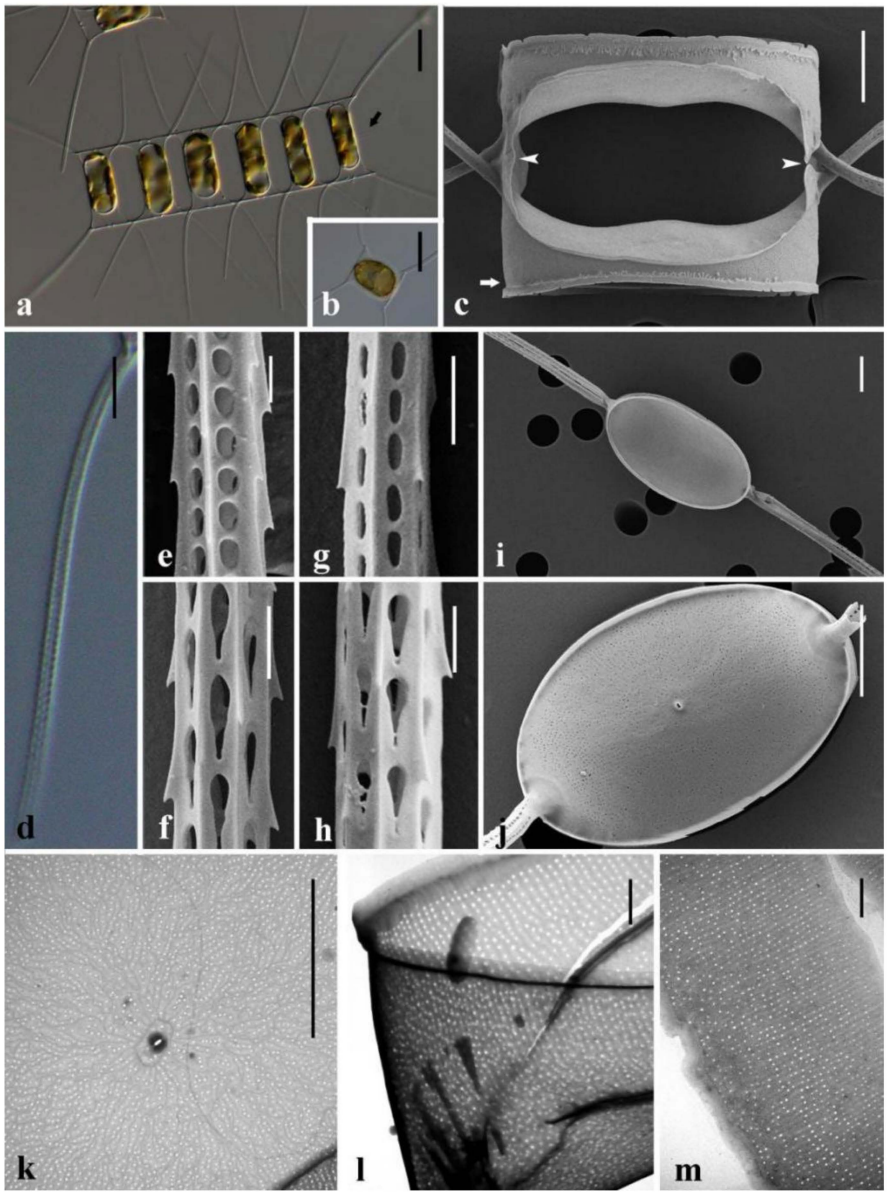

Figure 2. LM (**a**,**b**,**d**), SEM (**c**,**e**–**j**) and TEM (**k**–**m**) micrographs of vegetative cells of *Chaetoceros macroelegans* sp. nov., strain MC785. (**a**) Chains in broad girdle view, showing protrusions on terminal valve (arrow); (**b**) solitary cell; (**c**) sibling intercalary valves showing aperture, overlapping silica ear-like structures (arrowheads) and furrow above the basal ring of mantle (arrow); (**d**) terminal seta under LM, showing visible setae poroids; (**e**–**h**) setae structure, showing round-oval and tear-shaped poroids on terminal (**e**,**f**) and intercalary setae (**g**,**h**), respectively; (**i**) intercalary valve view; (**j**,**k**) terminal valves; (**l**) parallel rows of poroids on the mantle; (**m**) detail of bands. Scale bars: (**a**,**b**) 20 μm; (**c**,**d**,**i**–**k**) 5 μm; (**e**–**h**,**l**,**m**) 1 μm.

Diagnosis: Straight chains, sometimes solitary cells. Normally 4–10 chloroplasts in each cell. Apical axis 12.6–39.7 μm. Pervalvar axis 11.3–28.4 μm. Height of aperture 6.3–12.6 μm. Rectangular cells in girdle view. Central annulus, radiating costae and scattered poroids on valve face and mantle. Elliptical–hexagonal apertures. Setae Brunel I type. Short setae base or absent. Sibling setae intersect outside chain border without fusing. Tear-shaped and round-oval poroids on intercalary and terminal setae. Tear-shaped poroids 0.7–2.3 μm long on intercalary setae. Round-oval poroid density of 12–19 in 10 μm on terminal setae, 15–18 in 10 μm on intercalary setae. A single rimoportula with short external tube on the terminal valve. Several girdle bands marked by parallel rows of poroids and costae. Smooth resting

spores. Two elongated elevations with dichotomous branching processes on primary valve and one or two bulges on secondary valve.

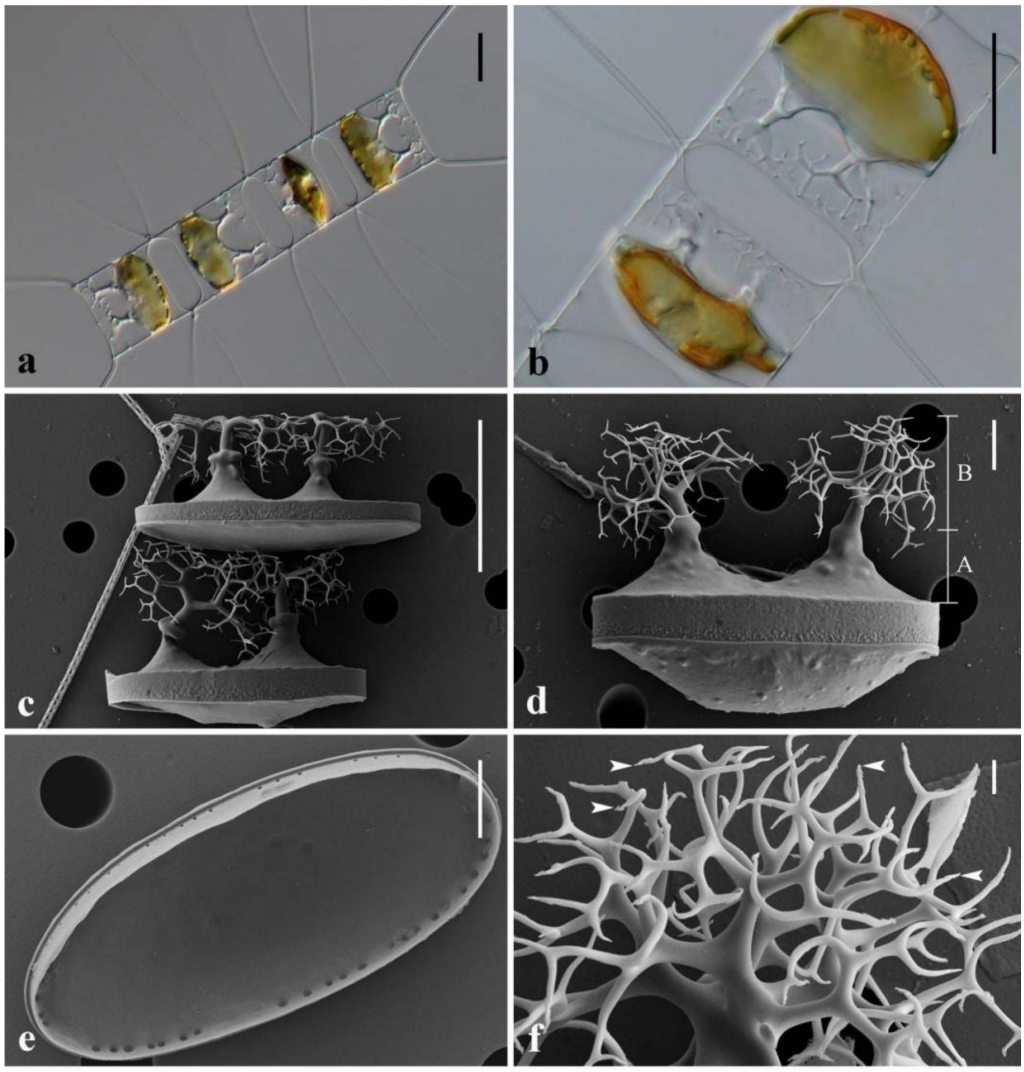

Figure 3. LM (**a**,**b**) and SEM (**c**–**f**) micrographs of resting spores of *Chaetoceros macroelegans* sp. nov., strain MC785. (**a**,**b**) Resting spores within mother cells; (**c**,**d**) released resting spores, showing two elongated elevations with dichotomous branching processes distally on the primary valve; A—height of elevation, B—height of branching process; (**e**) internal view of secondary valve; (**f**) hooks on the distal tips (arrowheads). Scale bars: (**a**–**c**) 20 µm; (**d**,**e**) 5 µm; (**f**) 1 µm.

Holotype: A permanent slide of strain MC785 is deposited at the Natural History Museum of Denmark, as C-A99707.

Isotype: Fixed material of strain MC785 deposited at the Marine Diatoms Collection of South China Normal University, as SN F-MC785, and a permanent slide of acid-washed material at the Natural History Museum of Denmark, as C-A99708.

Type locality: Ningbo coast (29.8636° N, 121.5611° E), East China Sea.

Etymology: *macro* refers the size of the tear-shaped poroids being larger on the intercalary setae than those in the two other species, and *elegans* refers the elegant outline of the chains, resembling the characteristics of *C. elegans*.

Registration: http://phycobank.org/103181.

Morphology: The chains are straight (Figure 2a), and solitary cells may occur (Figure 2b). Sometimes, non-silicified protrusions are visible centrally on the terminal valve in LM (Figure 2a, arrow); however, they disappear after acid cleaning. The cells are rectangular in broad girdle view, and the apical axis is usually longer than the pervalvar axis (Figure 2a,b).

The apertures are elliptical to hexagonal (Figure 2a), with slight constriction near the middle (Figure 2c).

The setae protrude from the valve corners, with short or no setae base (Figure 2a,c). All setae of a chain are located in the apical plane (Figure 2a,i, Brunel type I, [34]). In broad girdle view, the sibling setae form an acute angle and intersect outside the chain border (Figure 2c). The terminal setae form an open U shape (Figure 2a). The setae poroids, which are visible in LM (Figure 2d), usually form four or six longitudinal rows of poroids and spines arranged alternatingly (Figure 2e–h). The poroids are tear-shaped or round-oval on the terminal (Figure 2e,f) and intercalary setae (Figure 2g,h). Only one type of poroid can be observed on each seta, and there is no evident system determining which setae have tear-shaped or oval poroids. On the terminal setae, the tear-shaped poroids are 0.5–1.3 µm long with 11.0 ± 2.2 poroids in 10 µm, and the round-oval poroids are 0.4–0.6 µm long with 15.8 ± 2.3 poroids in 10 µm. On the intercalary setae, the tear-shaped poroids are 0.7–2.3 µm long with 7.9 ± 1.7 poroids in 10 µm, and the round-oval poroids are 0.4–0.5 µm long with 17.1 ± 1.2 in 10 µm (Table 2).

The valves are broadly elliptical (Figure 2i,j). The valve face is saddle-shaped, with a slightly raised central region (Figure 2c). On the valve face, a central annulus is surrounded by radiating costae with scattered poroids in between (Figure 2k). A single rimoportula with a short external tube is located centrally on the terminal valve (Figure 2j). On the intercalary valves, sibling cells show overlapping silica ear-like structures (Figure 2c) and a furrow is present above the basal ring of the mantle (Figure 2c). The mantle is decorated by parallel rows of poroids separated by costae (Figure 2l). Several open girdle bands are present, each band having parallel rows of poroids, which are separated by costae (Figure 2m). The apical axis is 12.6–39.7 µm, the pervalvar axis 11.3–28.4 µm, and the height of the apertures is 6.3–12.6 µm (Table 2).

The resting spores are formed centrally in the mother cells, touching the bands and sometimes the valves of the mother cell (Figure 3a,b). Valve surfaces are smooth. The primary valve possess two elongated elevations with dichotomous branching processes, and one or two bulges are present on the secondary valve face (Figure 3c,d). The angle of the outer slope of the elevation is acute. There is a ring of poroids on the mantle of the secondary valve (Figure 3e). Each process branches into a tree-like structure, with the distal tips pointed and possessing one or several hooks (Figure 3f). The elevations are 4.4–10.3 µm high, and the branching processes are 9.5–14.9 µm high (Table 2).

Geographical distribution: In the present study, it was sampled from the coastal waters off Hong Kong, Jiangmen, Zhuhai and Zhanjiang of the South China Sea, Ningbo of the East China Sea and Qingdao of the Yellow Sea (Table 1). This species has also been recorded as *C. elegans* in Guishan Island of the South China Sea (MC150 and MC153, [11]), New Brunswick, Canada (UNBF, [11]), Mannai Island in Thailand (M1, [11]), Xiamen of the East China Sea (MC1195, [35]) and the Taiwan Strait of the East China Sea (MC1166, [35]).

Chaetoceros densoelegans Lundholm & Yang Li sp. nov. (Figures 4 and 5).

Diagnosis: Straight chains, sometimes solitary cells. Apical axis 25.0–26.5 µm. Pervalvar axis 9.4–15.8 µm. Aperture in pervalvar axis 8.3–14.5 µm. Central annulus, radiating costae and scattered poroids on valve face and mantle. Elliptical–hexagonal apertures. Setae Brunel I type. Short setae base or absent. Sibling setae intersect outside chain border without fusing. Tear-shaped and round-oval setae poroids on intercalary and terminal setae. Tear-shaped poroids 0.6–0.9 µm long in intercalary setae. Round-oval poroid density of 15–27 in 10 µm in terminal setae, 13–27 in 10 µm in intercalary setae. A rimoportula, with short external process on the terminal valve. Several girdle bands decorated by parallel rows of poroids and costae. Smooth resting spores. Two elongated elevations with dichotomous branching processes on primary valve and one or two bulges on secondary valve.

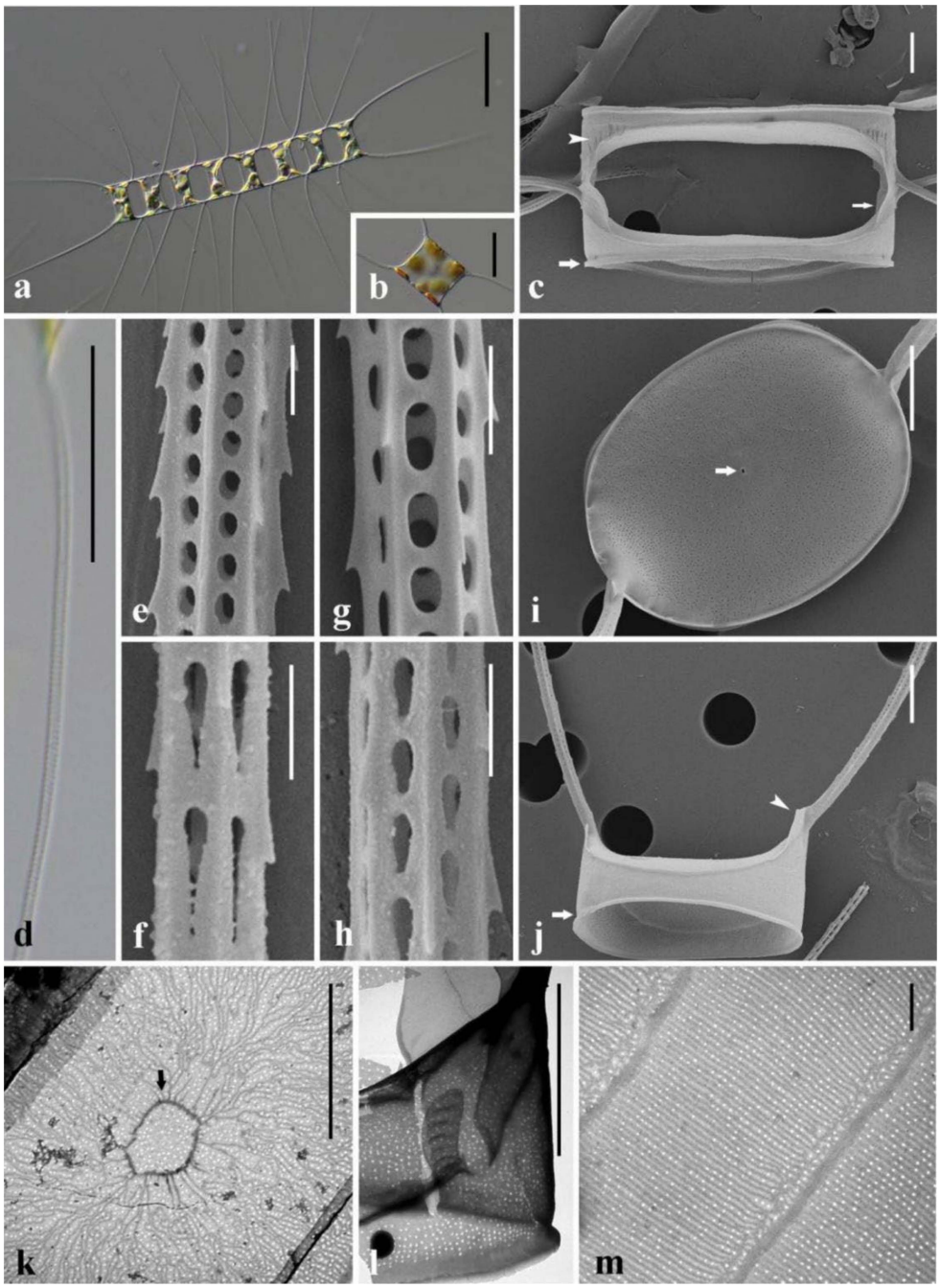

Figure 4. LM (**a**,**b**,**d**), SEM (**c**,**e**–**j**) and TEM (**k**–**m**) micrographs of vegetative cells of *Chaetoceros densoelegans* sp. nov., strain MC687. (**a**) Chain in broad girdle view; (**b**) solitary cell; (**c**) sibling intercalary valves showing aperture and overlapping silica ear-like structures (arrow), silica ridges (arrowhead) and furrow above the basal ring of mantle (broad arrow); (**d**) terminal seta under LM, showing visible setae poroids; (**e**–**h**) setae structure, showing round-oval and tear-shaped poroids on terminal (**e**,**f**) and intercalary setae (**g**,**h**), respectively; (**i**) terminal valve view showing external process of rimoportula (arrow); (**j**) terminal valves with silica ear-like structures (arrowhead) and furrow above the basal ring of mantle (arrow); (**k**) enlargement of intercalary valve, showing annulus (arrow), costae and poroids; (**l**) parallel rows of poroids on the mantle; (**m**) close-up of bands. Scale bars: (**a**,**b**,**d**) 20 μm; (**c**,**i**–**l**) 5 μm; (**e**–**h**,**m**) 1 μm.

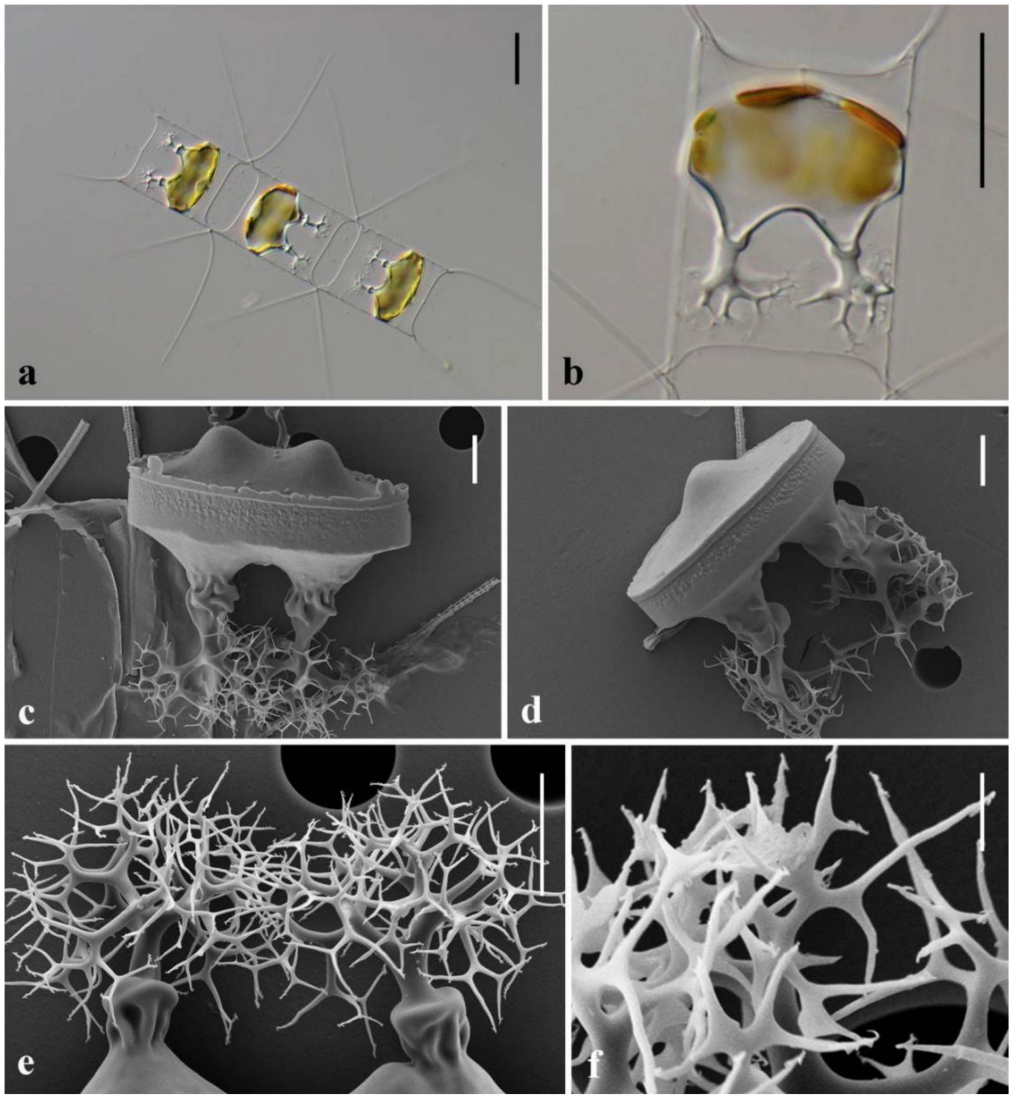

Figure 5. LM (**a**,**b**) and SEM (**c**–**f**) micrographs of resting spores of *Chaetoceros densoelegans* sp. nov., strain MC687. (**a**,**b**) Resting spores within mother cells of a chain; (**c**,**d**) released resting spores, showing two elongated elevations with dichotomous branching processes distally on the primary valve face and one (**d**) or two bulges (**c**) on the secondary valve face; (**e**) dichotomous branching processes; (**f**) hooks on the distal tips. Scale bars: (**a**,**b**) 20 µm; (**c**–**e**) 5 µm; 1 µm (**f**).

Holotype: A permanent slide of strain MC687 is deposited at the Natural History Museum of Denmark, as C-A99705.

Isotype: Fixed material of strain MC687 deposited at the Marine Diatoms Collection of South China Normal University, as SN F-MC687, and a permanent slide deposited at the Natural History Museum of Denmark, as C-A99706.

Type locality: Hong Kong (22.3520° N, 114.1139° E), South China Sea.

Etymology: *denso* refers to more densely spaced round-oval poroids on particularly the terminal setae than those in *C. macroelegans*, and *elegans* refers to the elegant outline of the chains, resembling the characteristics of *C. elegans*.

Registration: http://phycobank.org/103182.

Morphology: The chains are straight (Figure 4a), and sometimes solitary cells may occur (Figure 4b). The cells are rectangular in broad girdle view, and the apical axis is usually longer than the pervalvar axis (Figure 4a). The apertures are elliptical to hexagonal (Figure 4a,c).

The setae protrude from the valve corners, with a short or no setae base (Figure 4a,b). All setae of a chain are situated in the apical plane (Figure 4a, Brunel group I, [34]). In broad girdle view, the sibling setae form an acute angle and intersect outside the chain margin (Figure 4c). The terminal setae form a broad U shape (Figure 4a). The setae poroids are visible in LM (Figure 4d), and both tear-shaped and round-oval setae poroids are observed on the intercalary and terminal setae (Figure 4e–h). Only one type of poroid can be observed on each seta, and there is no evident system determining which setae have tear-shaped or oval poroids. On the terminal setae, the tear-shaped poroids are 0.5–0.7 µm long with 12.3 ± 2.7 poroids in 10 µm, and round-oval poroids are 0.2–0.5 µm long with 19.5 ± 3.1 poroids in 10 µm. On the intercalary setae, tear-shaped poroids are 0.6–0.9 µm long with 11.2 ± 2.1 poroids in 10 µm, and round-oval poroids are 0.3–0.5 µm long with 20.0 ± 4.2 poroids in 10 µm (Table 2).

The valves are broadly round-oval with a central external rimoportula process (Figure 4i). The valve face edge is broadly arc-shaped (Figure 4j) and a furrow is present above the basal ring of the mantle (Figure 4j). A central annulus, surrounded by radiating costae with scattered poroids in between, is present on the valve face (Figure 4k). The mantle is decorated by parallel rows of scattered poroids separated by costae (Figure 4l). Several open girdle bands are present, each ornamented by parallel rows of scattered poroids and costae (Figure 4m). The apical axis is 25.0–26.5 µm, the pervalvar axis 9.4–15.8 µm, and the height of the aperture is 8.3–14.5 µm (Table 2).

The resting spores are located centrally in the mother cells, touching the bands and sometimes the valves of the mother cell (Figure 5a,b). The surface of the resting spore is smooth. The primary valve possesses two elongated elevations with dichotomous branching processes, and one or two bulges are present on the secondary valve face (Figure 5c,d). Each process branches into a tree-like structure, with the distal tips pointed and possessing one or several hooks (Figure 5e,f). The elevations are 6.0–9.6 µm high, and the branching processes are 9.6–16.3 µm high (Table 2).

Geographical distribution: This species has been recorded as *C. elegans* in Concepción, Chile (strain Ch12A1) and Hong Kong [11].

3.2. Phylogenetic Analyses

In total, nine separate species are now known in the section *Dicladia* and, except for *C. lorenzianus*, for which verified molecular sequence data have been not recovered yet, all taxa in the section were included in the phylogenetic analyses. Similar tree topologies were inferred by the phylogenetic analyses of SSU and LSU rRNA and ITS gene sequences. *Chaetoceros laevisporus* and *C. mitra* made up the basal lineages in the section *Dicladia*, and *C. pauciramosus* appeared as a sister to a clade comprising *C. elegans*, *C. macroelegans* and *C. densoelegans* (Figures 6–8). The relationships among the three latter taxa varied slightly.

In the ITS tree (Figure 6), *C. macroelegans* and *C. densoelegans* were sister taxa and together they clustered with *C. elegans* in a well-supported clade (BI/ML, 1.00/89). No molecular divergences were found in *C. densoelegans* and *C. elegans* because all sequences of each species were identical, whereas 1–5 different base pairs differed among the strains of *C. macroelegans*. There were 38–41 different base pairs between *C. macroelegans* and *C. densoelegans*, whereas 52–56 and 56 base pairs differentiated *C. elegans* and *C. macroelegans*, *C. densoelegans*, respectively (Table S1).

In the SSU (Figure 7) and LSU analyses (Figure 8), *C. elegans*, *C. macroelegans* and *C. densoelegans* always clustered together, but the relationships differed slightly. In the SSU analyses (Figure 7), *C. macroelegans* was a sister taxon to *C. elegans* but not well supported. Meanwhile, in the LSU tree (Figure 8), *C. densoelegans* was sister to *C. elegans*, also not well supported. In the SSU analyses, two strains (MC777, MC785) made up a subclade in *C. macroelegans*, differing in one base pair from the remaining strains, whereas for *C. densoelegans* and *C. elegans*, the SSU sequences within each species were identical. In the LSU analyses, the sequences within each of the three species were identical. The number of base pair differences among the three taxa can be found in Tables S2 and S3.

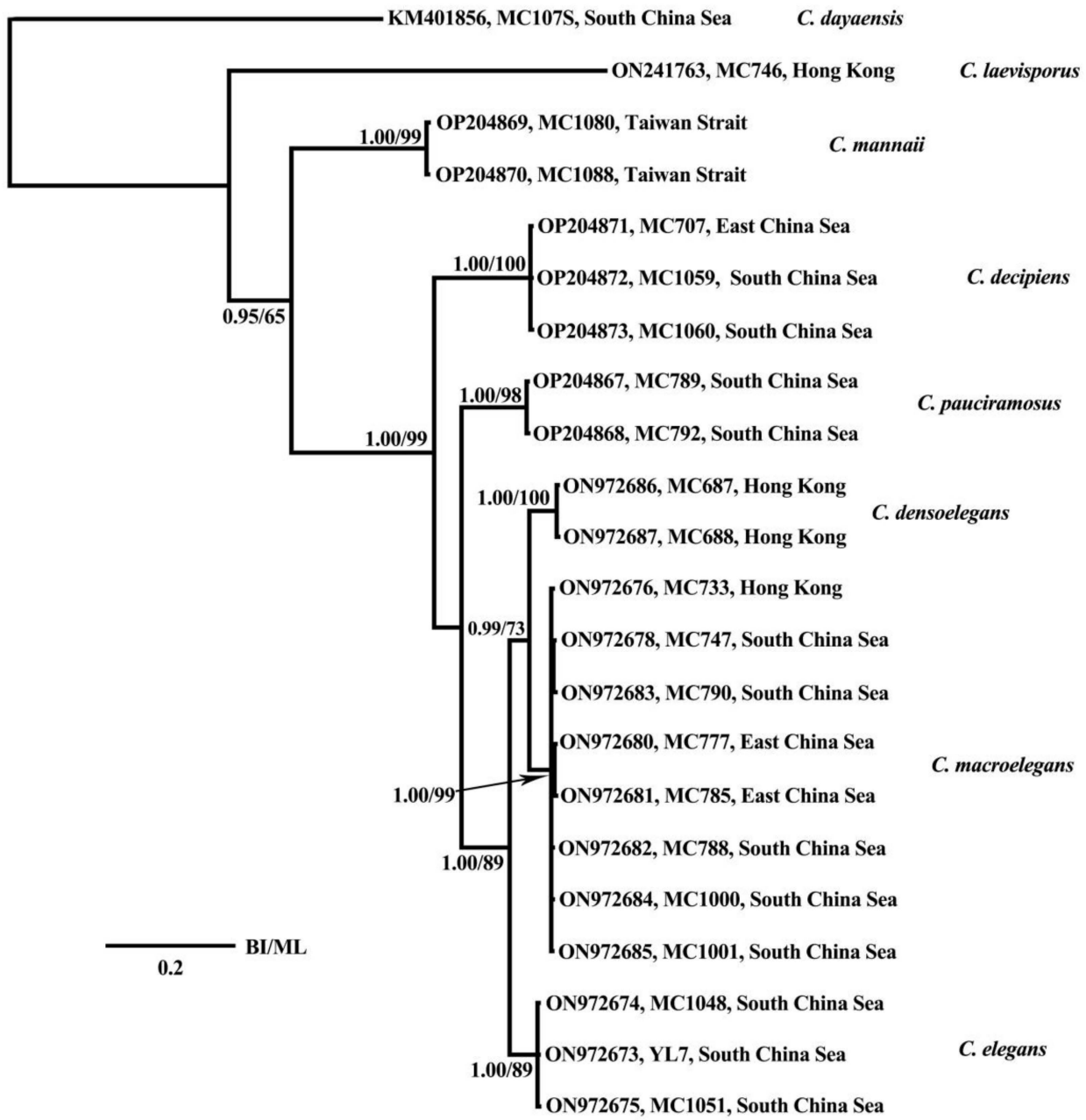

Figure 6. Phylogenetic tree based on maximum likelihood analyses of the ITS rDNA sequences. Only bootstrap support from Bayesian analyses (MrB) ≥0.95 and maximum likelihood (ML) ≥70% are shown.

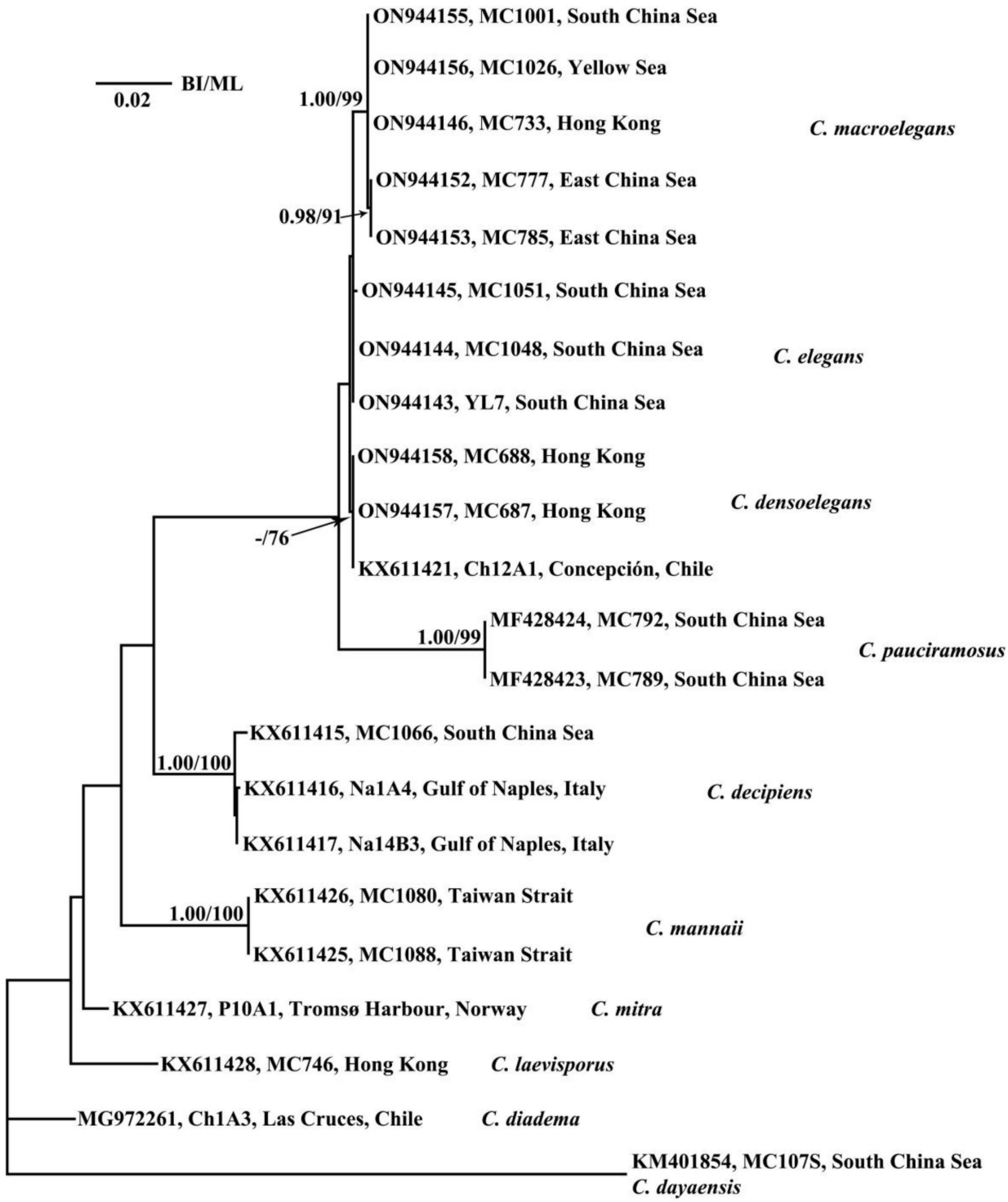

Figure 7. Phylogenetic tree based on maximum likelihood analyses of the SSU rDNA sequences. Only bootstrap support from Bayesian analyses (MrB) ≥0.95 and maximum likelihood (ML) ≥70% are shown.

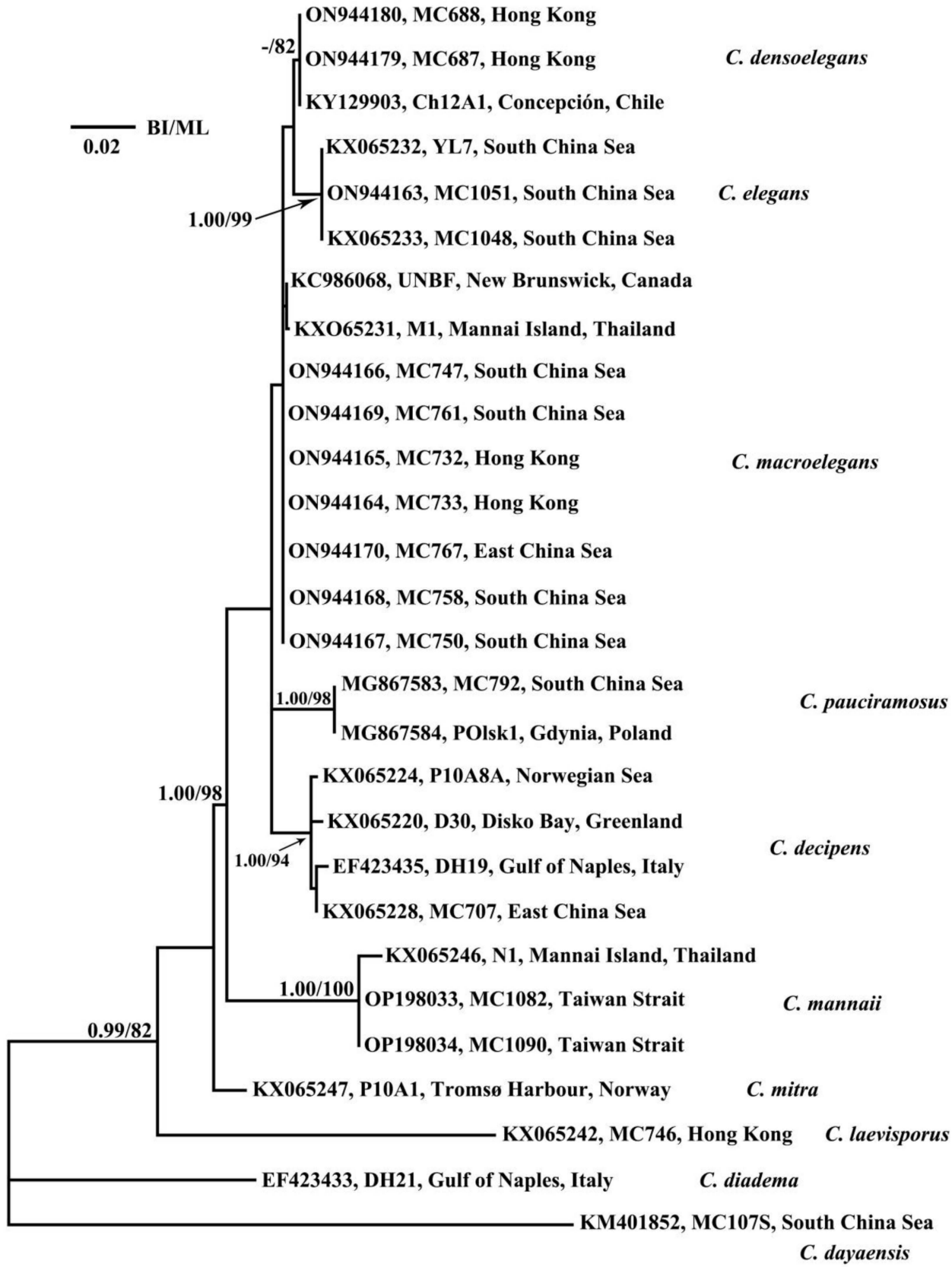

Figure 8. Phylogenetic tree based on maximum likelihood analyses of the LSU rDNA sequences. Only bootstrap support from Bayesian analyses (MrB) ≥0.95 and maximum likelihood (ML) ≥70% are shown.

3.3. CBC and HCBC Analyses

The ITS2 secondary structure of *C. elegans* included, as for other eukaryotes, four helices, with helix III as the longest, a universally conserved U-U mismatch (positions 94–95) in helix II and UGGU (positions 210–213) at the apex of helix III (Figure 9, [32]). When comparing the secondary structure of ITS2, *C. elegans* and *C. macroelegans* were distinguished by two CBCs and seven HCBCs (Figure 9), two CBCs in helix II (C-G:U-A, A-U:G-C), six HCBCs in helix III (A-U:G-U, G-U:A-U, G-U:G-C, G-C:G-U, U-G:U-A, U-A:U-G) and one HCBC in helix IV(U-G:C-G). There were four CBCs and eight HCBCs between *C. elegans* and *C. densoelegans* (Figure 9), two CBCs in helix II (C-G:U:A, A-U:G-C), one CBC (G-C:A-U) in helix III and one CBC (A-U:U-A) in helix IV, as well as one HCBC in helix IIa (G-U:A-U), six HCBCs (G-C:G-U, A-U:G-U, G-U:A-U, G-U:G-C, U-A:U-G, G-U:A-U) in helix III and one HCBC (U-G:C-G) in helix IV. Between *C. macroelegans* and *C. densoelegans*, no CBC but five HCBCs were found (Figure 9), one HCBC in helix IIa (G-U:A-U) and four HCBCs in helix III (G-C:G-U, G-U:A-U, U-A:U-G, G-U:A-U).

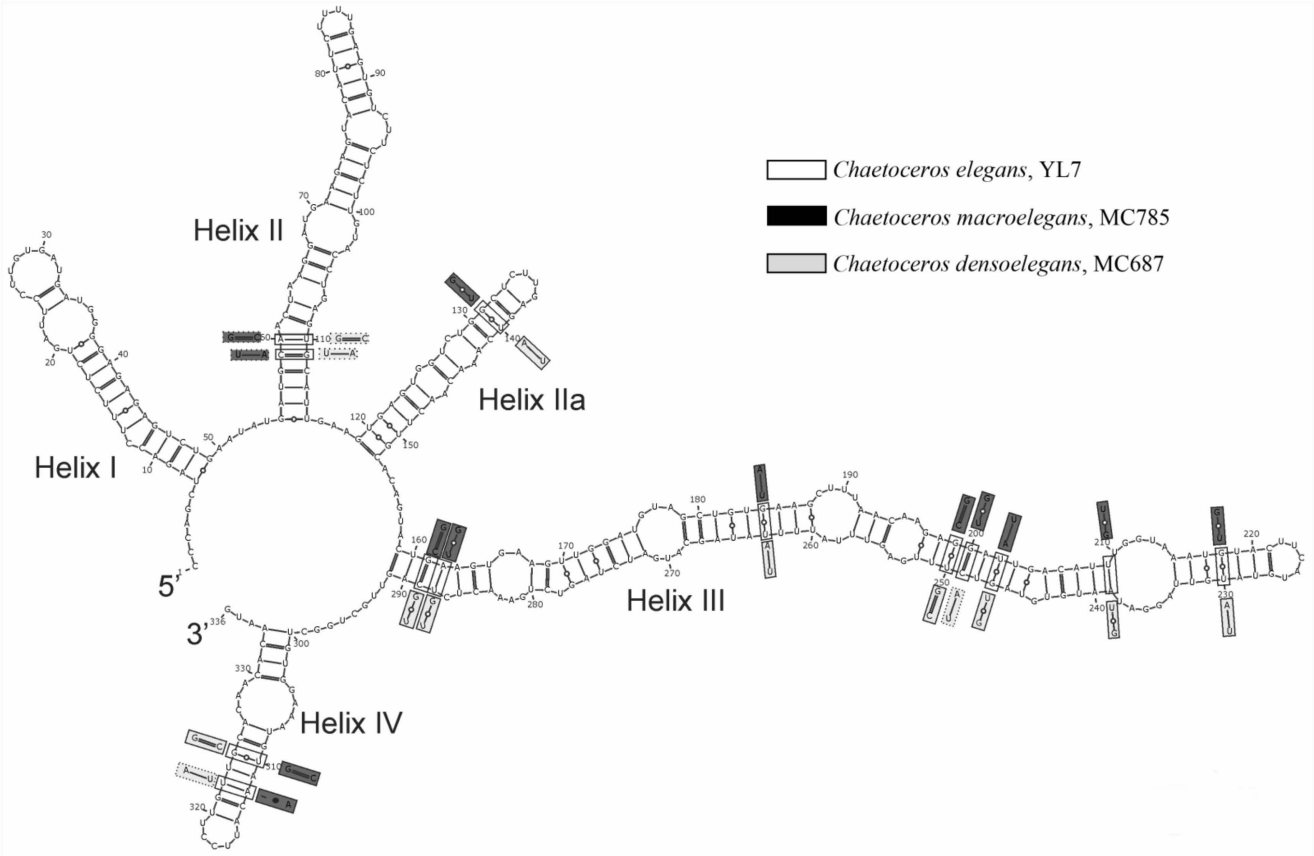

Figure 9. ITS2 RNA transcript of *Chaetoceros elegans* (strain YL7), with four common helices and one pseudo-helix II. CBCs and HCBCs between *C. elegans* and *C. macroelegans* (MC785), *C. densoelegans* (MC687) were indicated by rectangles, with dotted line and solid line, respectively. The base pairs of *C. elegans*, *C. macroelegans* and *C. densoelegans* are noted in white, black and grey, respectively.

4. Discussion

4.1. Taxonomic Positions of the New Taxa

All taxa in the section *Dicladia*, also known as the *C. lorenzianus* complex, formed a monophyletic lineage inferred from the three ribosomal genes used in the present study, confirming a recent validation of the section by a five multigene phylogeny [13]. The section has been characterized as having (1) straight chains with stiff setae, (2) normally 4–10 chloroplasts per cell, (3) setae with large poroids, (4) similar intercalary setae and diverging terminal setae, (5) resting spores, when known, with two elevations armed with

small branches on the primary valves [11,12]. In agreement with these morphological characteristics, *C. macroelegans* and *C. densoelegans* belong to the section *Dicladia*, which was also supported by the phylogenetic analyses (Figures 6–8).

Phylogenetically, the two new taxa always clustered in separate monophyletic clades, and always together with *C. elegans* in a larger common clade. At least two CBCs of the ITS2 secondary structure differentiated *C. elegans* from both *C. macroelegans* and *C. densoelegans* (Figure 9). Morphologically, the three taxa are similar, but smaller differences are seen in the basal parts of the setae and the shape, size and density of the setae poroids (see below). Based on the molecular and morphological differences, and supported by the presence of five HCBCs between *C. macroelegans* and *C. densoelegans*, two new taxa are described. Hence, the section *Dicladia* now comprises nine separate species.

4.2. Detailed Comparison of the Three Taxa

The three taxa, *C. elegans*, *C. macroelegans* and *C. densoelegans*, differ only in a few morphological characteristics. The presence of tear-shaped setae poroids has so far only been found in these three species in the *C. lorenzianus* complex. In *C. elegans*, only tear-shaped setae poroids were observed (Figure 1c–f), whereas both tear-shaped and round-oval setae poroids were seen in *C. macroelegans* and *C. densoelegans* (Figures 2e–h and 4e–h, respectively). In *C. elegans*, the tear-shaped poroids on the terminal setae were slightly larger (0.9 ± 0.2 µm vs. 0.7 ± 0.2 µm) and less densely spaced (9.4 ± 1.7 vs. 12.0 ± 3.1 in 10 µm) than those on the intercalary setae. In contrast, in *C. macroelegans*, the terminal setae possessed smaller and denser tear-shaped poroids (0.7 ± 0.2 µm, 11.0 ± 2.2 in 10 µm) than the intercalary setae (1.2 ± 0.3 µm, 7.9 ± 1.7 in 10 µm), whereas the size and density of the round-oval poroids were similar on both terminal and intercalary setae. Similar characteristics were seen in *C. densoelegans* (Table 2 and Table S4). Differentiating the two new species, the tear-shaped poroids on the intercalary setae were smaller in size and arranged with a higher density in *C. densoelegans* than in *C. macroelegans*. Finally, the density of the oval-round poroids was higher in *C. densoelegans* than in *C. macroelegans,* particularly on the terminal setae. Apart from the setae poroids, the setae base was distinct in *C. elegans* and the apertures were large and rounded quadrangular (Figure 1a,b), whereas the setae base was short or absent and the apertures were usually elliptical to rectangular in the other two taxa (Figure 2a,c and Figure 4a,c).

Resting spores are considered one of the key characteristics in the taxonomy of *Chaetoceros* [36]. In the present study, resting spores with two elongated elevations armed with complicated branches on the primary valves were found in *C. macroelegans* and *C. densoelegans*, whereas resting spores are still unknown in *C. elegans*. The resting spores reported in [11] (loc. cit. Figure 7a–f) do not characterize *C. elegans*, but belong to *C. macroelegans* and *C. densoelegans*, as the strains (MC785 and Ch12A1) were re-identified. For more morphological comparisons among the three species, see Table 2. The morphological differences between the three taxa are supported by molecular data. When comparing the ITS2 secondary structure, *C. macroelegans* and *C. densoelegans* differed from *C. elegans* by having two CBCs and four CBCs, or seven HCBCs and eight HCBCs, respectively (Figure 7), whereas the two new taxa only differed by five HCBCs and no CBC. Similarly, closely related species of morphologically more distinctly different diatom species have previously been differentiated by HCBC [37,38]. Along with the phylogenetic and morphological support, the secondary structure analyses of ITS2 support the description of the new taxa.

4.3. Comparing the Three Taxa in This Study with Close Species in the C. lorenzianus Complex

The presence of tear-shaped setae poroids is, as mentioned above, a unique feature, differentiating the three taxa from other allied taxa. Furthermore, poroids exist on the valve face and the mantle in the three taxa, but not in *C. laevisporus*, *C. mannaii* and *C. mitra* [11,12]. The external tube of the rimoportula is more distinct in *C. mannaii* than in all other taxa [12]. *Chaetoceros mitra* is unique by having the smallest size of setae poroids arranged into the densest pattern within the *C. lorenzianus* complex, 0.2 ± 0.1 µm, and a density of 39.8 ± 7.4

in 10 µm. Moreover, the intercalary sibling setae is Brunel II in *C. mitra*, each diverging 30–80° from the apical plane (loc. cit. Figure 13a,b, [11]), whereas it is always Brunel I in all the other species. *Chaetoceros elegans* is differentiated by the setae extending initially in the pervalvar axis, before curving and crossing over (Figure 1a,b). Thus, the seta base is distinct in *C. elegans*, whereas it is shorter or absent in all other species. *Chaetoceros elegans* is also unique by having rounded–quadrangular apertures, in contrast to oval–rectangular or peanut-shaped apertures in the other taxa. Finally, *C. macroelegans* has the largest size of tear-shaped setae poroids arranged with the lowest density in the *C. lorenzianus* complex. For further morphological comparisons, see Table S4.

The morphology of resting spores has been considered a unique feature of the *C. lorenzianus* complex, with spores having two elongated elevations on the primary valve and one or two bulges on the secondary valve face [20]. In this study, similar resting spores were reported in *C. macroelegans* and *C. densoelegans*, but are unknown so far in *C. elegans*. Presently, six species within the *C. lorenzianus* complex are known to possess resting spores, i.e., *C. laevisporus*, *C. mitra*, *C. pauciramosus*, type *C. lorenzianus*, *C. macroelegans* and *C. densoelegans*. The morphological comparisons of the resting spores made by [12] are still valid, except that *C. elegans* should be replaced by *C. macroelegans* and *C. densoelegans*, as no morphological differences in resting spore morphology were observed between the two new taxa (Table 2). *Chaetoceros laevisporus* is distinct by the absence of dichotomous branching on the elevations on the primary valve 11]. The resting spores of *C. mitra* differ by the straight slope of the elevation [11], whereas it forms an acute angle in the two new taxa (Figures 3 and 5). The resting spores in *Chaetoceros pauciramosus* are most similar to those in *C. macroelegans* and *C. densoelegans*, and no morphological differences were found. Resting spores with two branching processes have also been reported in *C. lorenzianus*, but the delineation of this taxon is still unclear and needs modification based on type material or samples from the type locality [11].

The identification and taxonomy of the genus *Chaetoceros* has, to a large degree, been based on light microscopical characteristics, such as the morphology of the chains, orientation of the setae, etc. However, these features are prone to change due to environmental factors or life stages, and should be used carefully (own observations). Recently, the ultrastructure on the setae, including the shape, size and arrangement of poroids and spines, the presence or absence of poroids on the valve face and mantle, morphology of resting spores, etc., has been shown to be useful for taxonomic delineations of taxa [2,3,7,9–11,39,40]. The shape of the setae poroids is quite unique in *C. elegans*, *C. macroelegans* and *C. densoelegans*, and differentiates them from not only the other taxa in the *C. lorenzianus* complex, but also from most *Chaetoceros* species. The ultrastructure on the setae and the characteristics of the resting spores were shown to have significant taxonomic importance in the present study and should be explored in more detail in the other *Chaetoceros* sections.

Supplementary Materials: The following supporting information can be downloaded at: https://www.mdpi.com/article/10.3390/d14080676/s1, Table S1: The number of base pair differences of ITS rDNA within *C. elegans*, *C. macroelegans* and *C. densoelegans* strains; Table S2: The number of base pair differences of SSU rDNA within *C. elegans*, *C. macroelegans* and *C. densoelegans* strains; Table S3: The number of base pair differences of LSU rDNA within *C. elegans*, *C. macroelegans* and *C. densoelegans*; Table S4: Morphological characters for differentiating the known nine species of the section *Dicladia*.

Author Contributions: Conceptualization, Y.L.; Data curation, X.C., Z.C. and X.X.; Formal analysis, X.C. and Y.L.; Funding acquisition, Y.L.; Investigation, Z.C. and X.X.; Methodology, X.C.; Resources, Z.C.; Software, S.T.T.; Supervision, Y.L.; Visualization, N.L. and Y.L.; Writing—original draft, X.C. and Y.L.; Writing—review & editing, N.L. and Y.L. All authors have read and agreed to the published version of the manuscript.

Funding: This work was supported by grants from the National Nature Science Foundation of China (32170206) and the Science and Technology Basic Resources Investigation Program of China (2018FY100200).

Institutional Review Board Statement: Not applicable.

Informed Consent Statement: Not applicable.

Data Availability Statement: All the data from the study is included in this manuscript.

Conflicts of Interest: Authors declare no conflict of interest.

References

1. Guiry, M.D.; Guiry, G.M. AlgaeBase. World-Wide Electronic Publication, National University of Ireland, Galway. Available online: http://www.algaebase.org (accessed on 10 January 2022).
2. Chamnansinp, A.; Li, Y.; Lundholm, N.; Moestrup, Ø. Global diversity of two widespread, colony-forming diatoms of the marine plankton, *Chaetoceros socialis* (syn. *C. radians*) and *Chaetoceros gelidus* sp. nov. *J. Phycol.* **2013**, *49*, 1128–1141. [CrossRef] [PubMed]
3. Chamnansinp, A.; Moestrup, Ø.; Lundholm, N. Diversity of the marine diatom *Chaetoceros* (Bacillariophyceae) in Thai waters-revisiting *Chaetoceros compressus* and *Chaetoceros contortus*. *Phycologia* **2015**, *54*, 161–175. [CrossRef]
4. Xu, X.J.; Lundholm, N.; Li, Y. A study of *Chaetoceros debilis* sensu lato species (Bacillariophyceae), with emendation of *C. debilis* and description of *C. galeatus* sp. nov. *J. Phycol.* **2020**, *56*, 784–797. [CrossRef] [PubMed]
5. Li, Y.; Lundholm, N.; Moestrup, Ø. *Chaetoceros rotosporus* sp. nov. (Bacillariophyceae), a species with unusual resting spore formation. *Phycologia* **2013**, *52*, 600–608. [CrossRef]
6. Li, Y.; Zhu, S.; Lundholm, N.; Lü, S. Morphology and molecular phylogeny of *Chaetoceros dayaensis* sp. nov. (Bacillariophyceae), characterized by two 90° rotations of the resting spore during maturation. *J. Phycol.* **2015**, *51*, 469–479. [CrossRef]
7. Gaonkar, C.C.; Kooistra, W.H.C.F.; Lange, C.B.; Montresor, M.; Sarno, D. Two new species in the *Chaetoceros socialis* complex (Bacillariophyta): *C. sporotruncatus* and *C. dichatoensis*, and characterization of its relatives, *C. radicans* and *C. cinctus*. *J. Phycol.* **2017**, *53*, 889–907. [CrossRef]
8. Kaczmarska, I.; Sammanta, B.; Ehrman, J.M.; Porcher, E.M.A. Auxosporulation in *Chaetoceros acadianus* sp. nov. (Bacillariophyceae), a new member of the section *Compressa*. *Eur. J. Phycol.* **2019**, *54*, 206–221. [CrossRef]
9. Xu, X.J.; Chen, Z.Y.; Lundholm, N.; Li, Y. Diversity in the section *Compressa* of the genus *Chaetoceros* (Bacillariophyceae), with description of two new species from Chinese warm waters. *J. Phycol.* **2019**, *55*, 104–117. [CrossRef]
10. Xu, X.J.; Lundholm, N.; Chen, Z.Y.; Li, Y. Revisiting section *Compressa* of *Chaetoceros* (Bacillariophyceae), with descriptions of *C. brevispinosus* sp. nov. and *C. ornatus* comb. nov. *Phycologia* **2019**, *58*, 614–627. [CrossRef]
11. Li, Y.; Boonprakob, A.; Gaonkar, C.C.; Kooistra, W.H.C.F.; Lange, C.B.; Hernández-Becerril, D.; Chen, Z.Y.; Moestrup, Ø.; Lundholm, N. Diversity in the globally distributed diatom genus *Chaetoceros* (Bacillariophyceae): Three new species from warm-temperate waters. *PLoS ONE* **2017**, *12*, e0168887. [CrossRef]
12. Chen, Z.Y.; Lundholm, N.; Moestrup, Ø.; Kownacka, J.; Li, Y. *Chaetoceros pauciramosus* sp. nov. (Bacillariophyceae), a widely distributed brackish water species in the *C. lorenzianus* complex. *Protist* **2018**, *169*, 615–631. [CrossRef] [PubMed]
13. De Luca, D.; Sarno, D.; Piredda, R.; Kooistra, W.H.C.F. A multigene phylogeny to infer the evolutionary history of *Chaetocerotaceae* (Bacillariophyta). *Mol. Phylogenet. Evol.* **2019**, *140*, 106575. [CrossRef] [PubMed]
14. Gaonkar, C.C.; Piredda, R.; Minucci, C.; Mann, D.; Montresor, M.; Sarno, D.; Kooistra, W.H.C.F. Annotated 18S and 28S rDNA reference sequences of taxa in the planktonic diatom family *Chaetocerotaceae*. *PLoS ONE* **2018**, *13*, e0208929. [CrossRef] [PubMed]
15. Guillard, R.L.; Hargraves, P.E. *Stichochrysis immobilis* is a diatom, not a chrysophyte. *Phycologia* **1993**, *32*, 234–236. [CrossRef]
16. Kraus, D. Daniel's XL Toolbox Addin for Excel, Version 6 October 2014. 2014. Available online: http://xltoolbox.sourceforge.net (accessed on 7 April 2022).
17. Anonymous. Proposals for a standardization of diatom terminology and diagnoses. *Nova Hedwig. Beih.* **1975**, *53*, 323–354.
18. Rines, J.E.B.; Hargraves, P.E. The *Chaetoceros* Ehrenberg (Bacillariophyceae) flora of Narragansett Bay, Rhode Island, USA. *Bibl. Phycol.* **1988**, *79*, 5–196.
19. Suto, I. Taxonomy of the marine resting spore genera *Dicladia* Ehrenberg, *Monocladia gen.* nov. and *Synendrum* Ehrenberg and their stratigraphic significance in Miocene strata. *Diatom Res.* **2003**, *18*, 331–356. [CrossRef]
20. Ishii, K.I.; Iwataki, M.; Matsuoka, K.; Imai, I. Proposal of identification criteria for resting spores of *Chaetoceros* species (Bacillariophyceae) from a temperate coastal sea. *Phycologia* **2011**, *50*, 351–362. [CrossRef]
21. Lundholm, N.; Daugbjerg, N.; Moestrup, Ø. Phylogeny of the Bacillariaceae with emphasis on the genus *Pseudo-nitzschia* (Bacillariophyceae) based on partial LSU rDNA. *Eur. J. Phycol.* **2002**, *37*, 115–134. [CrossRef]
22. Scholin, C.A.; Herzog, M.; Sogin, M.; Anderson, D.M. Identification of group- and strain-specific genetic markers for globally distributed *Alexandrium* (Dinophyceae). II. Sequence analysis of a fragment of the LSU rDNA. *J. Phycol.* **1994**, *30*, 999–1011. [CrossRef]
23. Nunn, G.B.; Theisen, B.F.; Christensen, B.; Arctander, P. Simplicity-correlated size growth of the nuclear 28S ribosomal RNA D3 expansion segment in the crustacean order Isopoda. *J. Mol. Evol.* **1996**, *42*, 211–223. [CrossRef] [PubMed]
24. Zhen, Y.; Mi, T.Z.; Yu, Z.G. Detection of *Phaeocystis globosa* using sandwich hybridization integrated with nuclease protection assay (NPA-SH). *J. Environ. Sci.* **2008**, *20*, 1481–1486. [CrossRef]
25. White, T.; Bruns, T.; Lee, S.; Taylor, J. Amplification and direct sequencing of fungal ribosomal RNA genes for phylogenetics. *PCR Protoc. A Guide Methods Appl.* **1990**, *18*, 315–322.

26. Hall, T.A. BioEdit: A user-friendly biological sequence alignment editor and analysis program for window 95/98/NT. *Nucleic Acids Symp.* **1999**, *41*, 95–98.
27. Stamatakis, A. RAxML-VI-HPC: Maximum likelihood-based phylogenetic analyses with thousands of taxa ad mixed models. *Bioinformatics* **2006**, *22*, 2688–2690. [CrossRef]
28. Boc, A.; Diallo, A.B.; Makarenkov, V. T-REX: A web server for inferring, validating and visualizing phylogenetic trees and networks. *Nucleic Acids Res.* **2012**, *40*, 573–579. [CrossRef]
29. Ronquist, F.; Teslenko, M.; Mark, P.V. MrBayes 3.2: Efficient Bayesian inference and model choice across a large model space. *Syst. Biol.* **2012**, *61*, 539–542. [CrossRef]
30. Nylander, J.A.A. *MrModeltest v2. Program Distributed by the Author*; Evolutionary Biology Center, Uppsala University: Uppsala, Sweden, 2004.
31. Seibel, P.; Müller, T.; Dandekar, T.; Wolf, M. Synchronous visual analysis and editing of RNA sequence and secondary structure alignments using 4SALE. *BMC Res. Notes* **2008**, *1*, 91. [CrossRef]
32. Wolf, M.; Koetschan, C.; Müller, T. ITS2, 18S, 16S or any other RNA-simply aligning sequences and their individual secondary structures simultaneously by an automatic approach. *Gene* **2014**, *546*, 145–149. [CrossRef]
33. Teng, S.T.; Tan, S.N.; Lim, H.C.; Dao, V.H.; Bates, S.S.; Leaw, C.P. High diversity of *Pseudo-nitzschia* along the northern coast of Sarawak (Malaysian Borneo), with descriptions of *P. bipertita* sp. nov. and *P. limii* sp. nov. (Bacillariophyceae). *J. Phycol.* **2016**, *52*, 973–989. [CrossRef]
34. Brunel, J. Orientation of setae in the genus *Chaetoceros*, in regard to the apical axis. *J. Mar. Biol. Ass. India* **1972**, *14*, 315–327.
35. Chen, Z.Y.; Xu, X.J.; Zhu, S.Y.; Zhai, M.Y.; Li, Y. Species diversity and geographical distribution of the *Chaetoceros lorenzianus* complex along the coast of China. *Biodivers. Sci.* **2019**, *27*, 149–158.
36. Hasle, G.R.; Syvertsen, E.E. Marine diatoms. In *Identifying Marine Phytoplankton*; Tomas, C.R., Ed.; Academic Press: San Diego, CA, USA, 1997; pp. 5–385.
37. Amato, A.; Montresor, M. Morphology, phylogeny and sexual cycle of *Pseudo-nitzschia mannii* sp. nov. (Bacillariophyceae): A pseudo-cryptic species within the *P. pseudodelicatissima* complex. *Phycologia* **2008**, *47*, 487–497. [CrossRef]
38. Casteleyn, G.; Chepurnov, V.A.; Leliaert, F.; Mann, D.G.; Bates, S.S.; Lundhulm, N.; Rhodes, L.; Sabbe, K.; Vyverman, W. *Pseudo-nitzschia pungens* (Bacillariophyceae): A cosmopolitan diatom species? *Harmful Algae* **2008**, *7*, 241–257. [CrossRef]
39. Lee, S.D.; Park, J.S.; Yun, S.M.; Lee, J.H. Critical criteria for identification of the genus *Chaetoceros* (Bacillariophyceae) based on setae ultrastructure. I. Subgenus *Chaetoceros*. *Phycologia* **2014**, *53*, 174–187. [CrossRef]
40. Lee, S.D.; Joo, H.M.; Lee, J.H. Critical criteria for identification of the genus *Chaetoceros* (Bacillariophyceae) based on setae ultrastructure. II. Subgenus *Hyalochaete*. *Phycologia* **2014**, *53*, 614–638. [CrossRef]